



Published in final edited form as:

*Biomacromolecules*. 2009 October 12; 10(10): 2935–2944. doi:10.1021/bm9007452.

## Osteogenic differentiation of human mesenchymal stem cells directed by extracellular matrix-mimicking ligands in a biomimetic self-assembled peptide amphiphile nanomatrix

Joel M. Anderson<sup>†</sup>, Meenakshi Kushwaha<sup>†</sup>, Ajay Tambralli<sup>†</sup>, Susan L. Bellis<sup>†,‡</sup>, Renato P. Camata<sup>§</sup>, and Ho-Wook Jun<sup>†,\*</sup>

<sup>†</sup> Department of Biomedical Engineering, University of Alabama at Birmingham, Birmingham, AL 35233

<sup>‡</sup> Department of Physiology & Biophysics, University of Alabama at Birmingham, Birmingham, AL 35233

<sup>§</sup> Department of Physics, University of Alabama at Birmingham, Birmingham, AL 35233

### Abstract

This study investigated the ability of nanoscale, biomimetic peptide amphiphile (PA) scaffolds inscribed with specific cellular adhesive ligands to direct the osteogenic differentiation of human mesenchymal stem cells (hMSCs) without osteogenic supplements. PA sequences were synthesized to mimic the native bone extracellular matrix (ECM), expressing different isolated ligands (i.e. RGDS, DGEA, KRSR). All PAs were presented as self-assembled two-dimensional coatings for the seeded hMSCs. Initial attachment results demonstrated that the different PAs could be individually recognized based on the incorporated adhesive ligands. Long-term studies assessed osteogenic differentiation up to 35 days. The RGDS-containing PA nanomatrix expressed significantly greater alkaline phosphatase (ALP) activity, indicating the early promotion of osteogenic differentiation. A progressive shift towards osteogenic morphology and positive staining for mineral deposition provided further confirmation of the RGDS-containing PA nanomatrix. Overall, the PA nanomatrix clearly has great promise for directing the osteogenic differentiation of hMSCs without the aid of supplements by mimicking the native ECM, providing an adaptable environment that allows for different adhesive ligands to control cellular behaviors. This research model establishes the beginnings of a new versatile approach to regenerate bone tissues by closely following the principles of natural tissue formation.

### Keywords

ECM; mesenchymal stem cells; bone tissue engineering; biomimetic material; RGD peptide

### Introduction

The shifting paradigm for regenerative medicine is to engineer a nanostructured environment that mimics the complex hierarchical order and self-assembled formation of native tissue. This

\*Corresponding author: Department of Biomedical Engineering, 806 Shelby Building, 1825 University Boulevard, Birmingham, AL 35233, United States. Tel.: +1 205 996 6938; fax: +1 205 975 4919. hwjun@uab.edu (H.W. Jun).

Supporting Information Available

(1) The percentage of positively detected mineralization per area after von Kossa staining. (2) Cell density of hMSCs on PA coatings throughout the long-term incubation. This material is available free of charge via the Internet at <http://pubs.acs.org>.

approach is emphasized by the ongoing research of biomimetic scaffolds that employ a bottom-up tissue engineering approach. To capture the self-assembling complexity required, bioactive scaffolds need to emulate the intrinsic properties of the extracellular matrix (ECM), which is an intricate meshwork of proteins and polysaccharides with great cellular influence.<sup>1</sup> Cell-ECM interactions directly regulate cell behaviors, such as cell proliferation, growth, survival, polarity, morphology, migration, and differentiation.<sup>1, 2</sup> Furthermore, different ECM molecules can selectively affect many types of signaling transduction pathways based on the ligand sequences present, including differentiation pathways.<sup>3</sup> Thus, biomimetic scaffolds can be tailored to precise tissue regenerative needs by incorporating specific cellular adhesive ligands. In particular, a biomimetic, self-assembling nanomatrix for bone regeneration is proposed to direct osteogenic differentiation without the additional aid of osteogenic supplements by taking advantage of these naturally occurring signaling processes.

To this effect, we have investigated a biomimetic nanomatrix scaffold composed of ECM-mimicking peptide amphiphiles (PAs), which self-assemble into higher order structures to support human mesenchymal stem cells (hMSCs). For this study, the hMSCs were isolated from bone marrow and provide unique, multipotent cells that have the capacity to propagate various types of mesenchymal tissues, such as muscle, connective tissue, and bone.<sup>4</sup> PAs are amphiphilic molecules consisting of a hydrophilic peptide segment coupled via an amide bond to a hydrophobic alkyl chain.<sup>5, 6</sup> The interchangeability within the amino acid sequences of PAs offers an inherent versatility for many potential regenerative applications. Numerous examples are present in the literature and range from directed biological response<sup>6-10</sup> to hybrid scaffolding for dual functionality<sup>11, 12</sup> to delivery of therapeutic factors.<sup>13-17</sup> Furthermore, the amphiphilic nature of the molecule allows for the formation of self-assembled structures, as the polar and apolar elements of the molecules tend to minimize entropically unfavorable interactions by aggregating together with the hydrophilic domains exposed to the outside and the hydrophobic sections remaining shielded within.<sup>18, 19</sup> The PAs for this study are designed to self-assemble into cylindrical nanofibers due to their conical shape, intertwining together to create an elaborate nanofiber meshwork that provides concurrent control of structure and biological functionality.<sup>20, 21</sup>

Past literature has presented conflicting evidence on osteogenic differentiation initiated by cell-ligand interactions without the presence of osteogenic supplements, such as dexamethasone,  $\beta$ -glycerol phosphate, ascorbic acid, and/or bone morphogenetic protein. No conclusive results have emerged, even though differentiation has been studied on many different types of biomaterials in either the presence or absence of stimulatory factors. For example, the osteogenic differentiation of mesenchymal stem cells with soluble osteogenic factors added to the media has been carried out on hydrogels, denatured type I collagen, and self-assembling PAs.<sup>22-26</sup> Conversely, Shin *et al.* has been able to induce the osteogenic differentiation of rat MSCs seeded on hydrogels based only on the cellular adhesive ligand sequence and without dexamethasone and  $\beta$ -glycerol phosphate supplements.<sup>27</sup> Therefore, this study aims to fully investigate the hypothesis that biomimetic self-assembling PAs functionalized with cellular adhesive ligands can direct the osteogenic differentiation and other cellular behaviors of hMSCs based exclusively on cell-ligand interactions (Fig. 1).

Three different bioactive PAs were synthesized, each functionalized with a specific ligand signal, and the proper control PAs were also prepared to include either a scrambled or no cellular adhesive ligand sequence. The general structure consisted of a cell adhesive ligand isolated from ECM proteins, enzyme degradable site specific for matrix metalloproteinase-2 (MMP-2), and hydrophobic alkyl tail attached to the N-terminus of the peptide segment. Of the isolated ligands, RGDS (Arg-Gly-Asp-Ser) functions as a general cell adhesive sequence first developed by Pierschbacher and Rouslahti.<sup>28</sup> It facilitates integrin-mediated binding and can be found in many ECM molecules, such as fibronectin, laminin, and osteopontin.<sup>29, 30</sup>

DGEA (Asp-Gly-Glu-Ala) is a collagen type I adhesive peptide sequence and has exhibited specific binding for osteoblasts via the  $\alpha$ 2- $\beta$ 1 integrin.<sup>31</sup> The KRSR (Lys-Arg-Ser-Arg) sequence binds to transmembrane proteoglycans and has been found to selectively increase osteoblast adhesion when functionalized with other bioadhesive moieties.<sup>32, 33</sup> The other half of the peptide structure consisted of the amino acid sequence GTAGLIGQ (Gly-Thr-Ala-Gly-Leu-Ile-Gly-Gln), which is sensitive to MMP-2. This motif allows for cell-mediated proteolytic degradation of the nanofiber network, enabling cell migration through the matrix and eventual remodeling with natural ECM.<sup>8</sup>

The novel PAs were first synthesized and their ability to self-assemble into nanomatrix coatings was assessed. To evaluate the cell-ligand interactions within the nanomatrices, initial attachment, proliferation, and long-term osteogenic differentiation potential of the hMSCs on the different PA coating conditions were studied. The culture of hMSCs in osteogenic supplemented media was also included as a positive control for the long-term differentiation studies. The osteogenic differentiation was examined by cell morphology, osteogenic markers, and mineral deposition, and in all cases, the cellular responses to the PAs coatings were evaluated with no stimulatory factors present.

## Materials and methods

### Peptide amphiphile synthesis

All PAs were synthesized using standard Fmoc-chemistry on an Advanced Chemtech Apex 396 peptide synthesizer at a 0.30 mmol scale, similar to previously described syntheses.<sup>16, 21, 34, 35</sup> Alkylation was obtained by reacting *N*-termini of the peptides with 2 equivalents of palmitic acid, 2 equivalents of *o*-benzotriazole-*N,N,N',N'*-tetramethyluroniumhexafluorophosphate (HBTU), and 4 equivalents of diisopropylethylamine (DiEA) in dimethylformamide (DMF) for 12 hours at room temperature. After repeating the alkylation reaction once, cleavage and deprotection of the PAs were performed using a mixture of trifluoroacetic acid (TFA), deionized (DI) water, triisopropylsilane, and anisole in the ratio of 40:1:1:1 for 3 hours at room temperature. The resulting solution for each was filtered, and the resin was rinsed with 20 mL of TFA. The collected samples were rotoevaporated and then precipitated in cold ether. The precipitates were collected and dried under vacuum. PAs were analyzed for impurities by matrix-assisted laser desorption ionization time of flight (MALDI-TOF) mass spectrometry.

### Formation of self-assembled peptide amphiphile nanofiber coatings

A 0.1% wt. stock solution for each PA was prepared in DI water and adjusted to pH 7.4 by the addition of NaOH. From this PA stock solution, 200  $\mu$ L per well were placed in 8-well silicone flexiPERM cell-culture chambers attached to glass cover slides. The chambers were placed in a chemical fume hood for 24 hours to evaporate the solvents and induce self-assembly. PA coatings were dried for two days in a 37°C incubator.

### Transmission electron microscope (TEM) imaging

A 5  $\mu$ L sample of each 0.1% wt. PA solution was applied to a carbon coated formvar cooper grid (400 mesh) and dried for 24 hours beforehand in a chemical fume hood to induce solvent evaporation self-assembly. The grids were negative stained with 10  $\mu$ L of 20% phosphotungstic acid (PTA) buffered to pH 7 for 30 seconds before wicking off the excess. The samples were examined on a Tecnai T12 microscope by FEI operated at a 60 kV accelerating voltage.

## Cell culture

hMSCs isolated from bone marrow were purchased from Lonza, Inc. (Walkersville, MD). hMSCs within passage number 3 – 6 were used for all experiments and grown with either normal or osteogenic culture media. Normal culture media included: Dulbecco's Modified Eagle's Medium (DMEM; Mediatech, VA) prepared with 10% fetal bovine serum (FBS; HyClone, UT), 1% Amphotericin B, 1% penicillin, and 1% streptomycin (Mediatech, VA). The osteogenic media consisted of normal culture media supplemented with 100 nM dexamethasone, 10 mM  $\beta$ -glycerol phosphate, and 0.05 mM ascorbic acid (Sigma Aldrich, MO). The PA coated 8-well flexiPERM cell-culture chambers were UV sterilized (254 nm, 172.8 kJ/cm<sup>2</sup>) for 4 hours so as not to affect the peptide-based samples. The hMSCs were lifted using 0.05% trypsin/EDTA solution and re-suspended with normal culture media at a concentration of 300,000 cells/mL. A cell suspension of 100  $\mu$ L (37,500 cells/cm<sup>2</sup>) was seeded onto each PA coated culture chamber well. Cell cultures were maintained under standard culture conditions (37°C, 95% relative humidity, and 5% CO<sub>2</sub>) with the media changes every 3–4 days. At given time points, the samples were removed and stored at –80°C. All collected samples were analyzed together for each biochemical assay.

## Sample preparation for assays

Samples were prepared for measuring cellularity and ALP activity in the following manner. After 1 and 4 hours and on days 7, 14, and 21, the cultured layers of hMSCs were washed with PBS and incubated for 30 minutes at 37°C with 0.25% trypsin. The phenol red was removed from the trypsin to prevent any colorimetric interference. The efficiency of removing the trypsinized cells was visually verified for each surface coating, as virtually all had been collected from each well. The collected cell samples were diluted with PBS at a 1:1 ratio and immediately stored at –80°C. On the day of each assay, the collected cell samples were lysed by a thaw/freeze cycle (30 minutes thawing at room temperature, 15 minutes of sonication, freezing at –80°C for 1 hour).

## Analysis of cellularity

The cell attachment for each time point was measured using a fluorometric PicoGreen DNA kit (Molecular Probes, OR) that quantifies the amount of double stranded DNA in cells. The fluorescent absorbance from the samples was measured using a microplate fluorescent reader (Synergy HT, BIO-TEK Instrument, VT) equipped with a 485/528 (EX/EM) filter set. A standard curve based on known concentrations of calf thymus DNA was used to determine the total amount of DNA. The cell number was calculated using  $7.88 \times 10^{-6}$   $\mu$ g of DNA/cell.

## Proliferating cell nuclear antigen (PCNA) staining

Self-assembled PA coatings were prepared on glass cover slides attached to 8-well silicone flexiPERM cell-culture chambers as described previously. hMSCs were seeded at 18,750 cells/cm<sup>2</sup> and incubated for 24 and 48 hours. At these two time points, the cells were fixed with 200  $\mu$ L of formalin for 10 minutes and then rinsed with PBS. 200  $\mu$ L of methanol were added for two minutes at room temperature to permeabilize the cells. After rinsing with PBS, the cells were incubated with 200  $\mu$ L of 3% hydrogen peroxide for 5 minutes at room temperature, again rinsed with PBS, and soaked with Tris buffered saline for 5 minutes to remove any excess. The primary anti-PCNA antibody (Dako Corp., CA) and secondary anti- mouse IgG HRP antibody (Dako Corp., CA) solutions were both prepared at 1:100 dilutions. The fixed cells were labeled with 200  $\mu$ L of the primary anti-PCNA antibody solution and incubated for 60 minutes at room temperature in a humidified chamber. After aspirating the antibody solution and rinsing with PBS, 200  $\mu$ L of the secondary anti-mouse IgG HRP antibody were added, followed by another 60 minute incubation period at room temperature in a humidified chamber. Chromogenic substrate solution prepared from an AEC kit (Invitrogen, CA) was added to each well in 200

$\mu\text{L}$  aliquots and incubated for 10 minutes. The samples were rinsed with PBS and counter stained with Mayer's hematoxylin (Dako Corp., CA) for 5 minutes. Repeated rinsing with 200  $\mu\text{L}$  of 37mM  $\text{NH}_4\text{OH}$  was performed until the solution turned blue, indicating removal of Mayer's hematoxylin excess. The stained samples were then mounted and viewed under a phase contrast microscope. To quantify the percentage of PCNA positive cells, 5 random fields from each PCNA stained culture chamber well were imaged, and the averaged ratio of proliferating cells compared to total cell number was calculated for each sample.

### Alkaline phosphatase (ALP) activity assay

Aliquots of 60  $\mu\text{L}$  cell lysates, 60  $\mu\text{L}$  alkaline buffer, and 100  $\mu\text{L}$  phosphatase substrate solutions were all added to a 96-well plate and incubated for 1 hour at 37°C. Standards in known concentrations ranging from 0 to 1000  $\mu\text{M}$  were prepared using p-nitrophenol and added to designated wells in the same plate. After incubating for 1 hour, the kinase reaction was stopped by adding 100  $\mu\text{L}$  of 0.3 M NaOH to each well. The absorbance of each well was measured using a microplate reader (EL  $\times$  800, BIO-TEK Instrument, VT) at 405 nm. The results were normalized to the total cell number at each time point measured by the PicoGreen DNA assay as previously described and displayed as the amount of p-nitrophenol produced per cell after 1 hour incubation.

### Mineral deposition

Before fixing the cells of each sample, the morphology was recorded with phase contrast microscope imaging at each time point, looking for characteristic signs of osteogenic differentiation. For von Kossa staining, the fixed cells were rinsed with 200  $\mu\text{L}$  of PBS, stained with 400  $\mu\text{L}$  of 5% silver nitrate, and exposed to UV light for 30 minutes. The reaction was stopped by adding 200  $\mu\text{L}$  of 5% sodium thiosulfate to each sample for 5 minutes at room temperature. The samples were rinsed to remove any excess stain and imaged under phase contrast microscopy. The area measurements of the positively stained mineral deposits were quantified with Adobe Photoshop CS4 (Adobe Systems, CA). Five or more images per coating condition at each time period were analyzed.

### Statistical analysis

All experiments were performed at least three times or more. The graphical results are representative data sets performed in quadruplicate. All values are expressed as means  $\pm$  standard deviation. SPSS 15.0 software (SPSS Inc., IL) was used to perform all statistical analysis. One-way analysis of variance (ANOVA) was used to assess significant differences. Tukey multiple comparisons test was also conducted to determine significant differences between pairs. For all statistical tests,  $p < 0.05$  was considered significant.

## Results

### Two-dimensional nanofiber self-assembly

All five PAs, including the controls, were successfully synthesized, as the molecular weight of each was verified by MALDI-TOF mass spectrometry (Table 1). TEM imaging was then used to characterize the self-assembled PA formations. Self-assembly was induced by evaporating the solvent from an aqueous PA solution (0.1% wt.) directly onto the chamber surface. This is in contrast with the more established self-assembly induction methods of adding divalent ions or lowering the pH.<sup>6,8,9</sup> As expected, TEM imaging in Fig. 2 demonstrated successful cylindrical micelle nanofiber self-assembly for all novel PA sequences with this two-dimensional coating method. The nanofibers imaged were similar in size to past literature, exhibiting a uniform diameter of approximately 6–10 nm and a length dimension at least 50-fold greater.<sup>21, 36</sup> At the microscale level, consistent multilayered nanofiber coatings were

found for each PA, demonstrating the uniformity of the self-assembled PA surface conditions. As depicted, each PA was able to self-assemble into numerous nanofiber meshworks stacked on top of each, thereby covering the entire surface area for all 2-D PA coatings. These self-assembled formations provided multilayered accessibility to the cell adhesive ligands or control sequences functionalized within the outer hydrophilic domains. Interestingly, other studies have used solvent evaporation induction methods, but none verified nanofiber self-assembly with TEM imaging or used the same PA sequences.<sup>37, 38</sup> This finding demonstrates that self-assembly of PAs can be achieved very simply by solvent evaporation, as the concentration of PAs reach the critical point needed for self-assembly.

First, the ability of the hMSCs to recognize the cell adhesive ligands within the PAs needed to be evaluated. This was accomplished with short-term studies characterizing the influence of the different cell-ligand interactions presented by the designed PAs. The initial cell attachment for 1 and 4 hours in Fig. 3 was significantly higher on the PA-RGDS coating compared to all the other PA coatings, as the values increased ~50% between hour 1 ( $20421.5 \pm 3967$ ) and hour 4 ( $36088.8 \pm 3485$ ). The PA-DGEA coating followed next, exhibiting significantly greater attachment than PA-KRSR, PA-RGES, and PA-S after 1 and 4 hours. Initial attachment to PA-KRSR essentially remained constant for 1 and 4 hours with values approximately half of PA-DGEA. The two control conditions of PA-RGES and PA-S also exhibited low attachment in the same range as PA-KRSR for both time points. Thus, the initial cell density is dependent on the inscribed signals present in the self-assembled PA coatings. This is similar to other studies where surfaces modified with RGDS-containing peptide sequences were found to exhibit greater cell attachment compared to DGEA, KRSR, or other control peptide sequences over short incubation periods.<sup>31, 39</sup>

### Quantification of PCNA staining

Proliferating cell nuclear antigen (PCNA) is a 36 kd protein prevalent during the S-phase of the cell cycle and has a well established correlation to cell proliferation.<sup>40, 41</sup>

Immunohistochemical labeling was used to evaluate hMSC proliferation on the different PA nanomatrices after 24 and 48 hours, as the percentage of positive PCNA stained cells compared to the total cell number was calculated for each sample (Fig. 4). For all PA nanomatrices, no significant differences in hMSC proliferation were observed at both time points. Each surface condition maintained a proliferation percentage between 30% – 60%, which is an expected amount of cells in the S-phase based on previous studies.<sup>42, 43</sup> This finding differs with the initial cell attachment results, which found cell density to be dependent on ligand signals. Thus, any differences observed during the long-term osteogenic differentiation studies cannot be attributed to proliferation and would most likely be due to the different cell-ligand interactions within the designed PA nanomatrices.

Alkaline phosphatase (ALP) is an enzyme that removes phosphate groups produced by osteoblasts. It is a widely used marker for osteoblast detection, and an increase in activity is associated with early osteogenic differentiation.<sup>44</sup> In Fig. 5, PA-RGDS showed significantly greater ALP activity than PA-DGEA, PA-KRSR, PA-RGES, and PA-S on days 14 ( $0.292 \pm 0.028$ ) and 21 ( $0.460 \pm 0.160$ ), respectively. Also, the ALP activity produced by PA-RGDS for days 14 and 21 increased significantly relative to day 7. The ALP activity of hMSCs on PA-DGEA continually increased up to day 14 ( $0.150 \pm 0.078$ ) before plateauing. The PA-KRSR coating maintained a similar ALP activity range as PA-DGEA, slowly increasing in value up to day 21. The ALP activity for PA-KRSR was found to be significantly more on day 21 compared to the days 7 and 14; however, the values still remained much lower compared to PA-RGDS. The same held true for both PA-RGES and PA-S, as no values of significance were observed on these control surfaces after 21 days. Based on these results, the ALP activity promoted by PA-RGDS was compared to hMSCs cultured on glass with or without osteogenic

supplemented media (OSM), as shown in the inset of Fig. 5. The addition of OSM produced approximately a five-fold increase in ALP activity over PA-RGDS, indicating that the ligand-driven osteogenic differentiation is in an earlier stage of maturation. While the RGDS ligand produced a less developed state compared to the level induced by supplemental factors, the overall data clearly demonstrates that the RGDS signaling peptide promotes greater osteogenic differentiation of hMSCs compared to all other PA coated surfaces.

### hMSC morphology during osteogenic differentiation

The cell morphology of the hMSCs was separately observed with phase contrast microscopy for to 35 days. In general, there are three distinct phenotypes observed over the course of osteogenic development: (1) proliferating, (2) matrix maturation, and (3) mineralization.<sup>45</sup> For hMSCs cultured on the five different PAs coatings plus glass as a reference, the most pronounced morphological changes were seen on the PA-RGDS coating, shown in Fig. 6(a–d). After the initial proliferating phase, the hMSCs cultured on PA-RGDS started to morphologically change from spindle-shaped to cuboidal or polygonal by day 14, becoming increasingly more apparent by day 21. By days 28 and 35, the cuboidal cells began to form large nodular colonies on PA-RGDS in an intermittent, island-like fashion. While the nodular colonies were not as uniformly distributed as the smaller clustered formations observed under OSM culturing (Fig. 6j), the shifted osteogenic appearances on PA-RGDS were very evident and much larger. Conversely, the PA-DGEA coating (Fig. 6e) was the only other surface condition to show signs of cell morphology change and colony clusters after 35 days. There were no such osteogenic appearances seen on the PA-KRSR culture samples (Fig. 6f). Likewise, the hMSCs cultured on the control surfaces of PA-RGES, PA-S, and glass (Fig. 6g–i) maintained an undifferentiated, spindle-shape morphology. Thus, the inscribed RGDS ligand signals appear to have the most impact on hMSC morphology when culturing without osteogenic supplements. This observed morphological shift and colony formation on the PA-RGDS nanomatrix compares favorably to the OSM cultured samples and indicates increased ECM production and subsequent mineral deposition, characteristic signs of osteogenic differentiation.<sup>45–48</sup>

### Mineral deposition

Mineral deposition in the cellular environment serves as a late stage marker, signifying complete osteogenic differentiation.<sup>49</sup> To investigate mineralization, von Kossa staining was used to qualitatively assess each of the PA nanomatrix coatings and glass controls, shown in Fig. 7. Significantly more mineral deposition (brownish-black precipitates) was detected on PA-RGDS than the other PA surface conditions, and the detected mineralized areas were comparable to the positively stained OSM cultured samples. Small mineralized deposits were detected on PA-DGEA after 35 days as well, but the stained nodules were not as pronounced and prevalent compared to PA-RGDS. No mineralized depositions were found on the PA-KRSR, PA-RGES, PA-S, and glass culture conditions.

Additionally, the numerous areas of positively stained mineral deposits on all culture conditions have been quantified (Fig. 8 and Supporting Information, Fig. S1). Significantly larger mineralized areas were observed on PA-RGDS and glass plus OSM, as both displayed the same general size range and percentage area of stained deposits. Furthermore, the positive mineralized areas found on PA-RGDS generally increased in size and area percentage between days 28 and 35, indicating a higher degree of mineralization. The PA-DGEA nanomatrix presented the only other quantifiable mineralization; however, the detected areas for this coating were considerably smaller in size. In addition to strongly correlating with the glass plus OSM condition, the positive mineral stains observed on PA-RGDS are similar to past findings that used osteogenic supplements to enhance mineralization on scaffolds functionalized with the RGDS epitope.<sup>50, 51</sup> Interestingly, evidence of mineral deposits was

only found on PA surface conditions displaying bioactive integrin-mediated ligands, as opposed to proteoglycan-mediated ligands. Overall, this demonstrates the importance of signaling peptides to mineral deposition and implies that the integrin-mediated RGDS ligand has the best capacity to direct later stage osteogenic development without the present of soluble factors.

## Discussion

Tissue engineering has many potential regenerative medicine applications and is constantly undergoing rapid change and development. Focusing on bone regeneration, the ideal strategy is to emulate the essential properties of the natural bone hierarchical structure using a bottom-up approach. Thus, a bone ECM-mimicking nanomatrix has been developed, consisting of self-assembling peptide amphiphiles synthesized with specific cell adhesive ligands that serve as a nanoscale interface for hMSCs to provide biological activity. The combination of promising cellular adhesive ligands with self-assembling nanomatrices creates a novel biomimetic material. This study investigated the ability of different cell adhesive ligands inscribed into the biomimetic PA nanomatrices to influence cellular behaviors due to the resulting cell-ligand interactions, which promote either integrin or non-integrin binding. The goal was to provide insight into directly controlling osteogenic differentiation based only on receptor mediated activation of the hMSCs by the cell adhesive ligand signals. Additionally, no aid from outside factors, such as media supplements or growth factors, was provided, divergent from almost all past osteogenic differentiation studies.

For all experiments, cell studies were conducted on two-dimensional PA nanomatrix coatings, created by solvent evaporation from an aqueous PA solution (0.1% wt.). After all the designed PAs were synthesized, self-assembly for each was successfully achieved by increased concentration and aggregation, as verified by TEM imaging. Consistent PA coating surfaces made up of multiple layers of nanofiber meshworks stacked on top of each other were found for all PA conditions, justifying that any experimental differences observed in cellular behavior were based on the cell adhesive ligands functionalized within the PA nanomatrix coatings. The influences of various cell adhesive ligands presented by the PA nanofibers were first tested with short-term cellular studies, focusing on initial attachment and proliferation. The PA-RGDS nanomatrix was found to be the best surface condition for initial hMSC attachment, demonstrating significantly more cell attachment after 1 and 4 hours than all the other coating conditions. PA-DGEA also showed greater cell attachment than PA-KRSR, PA-RGES, and PA-S at both time points. Conversely, cell proliferation analyzed by PCNA staining revealed no significant differences between the five PA nanomatrix coatings after 24 and 48 hours. Altogether, these results clearly prove that hMSCs can recognize and discern between the specific cell adhesive ligands incorporated into the PA nanomatrices during initial cell attachment, showing that these ligand signals are capable of eliciting different cellular responses. However, once the hMSCs are attached to the PA coatings, the seeded cells are able to proliferate at relatively the same rate, thereby setting an equal starting point for extended observations. Thus, these short-term experiments served as a gateway to evaluating osteogenic differentiation over longer incubation periods.

In the extended evaluations, the goal was to achieve osteogenic differentiation promoted only by the ligand-mediated bindings within the PA nanomatrix coatings. The ALP activity expressed by hMSCs after 21 days was used to initially assess differentiation, followed by an evaluation of cellular morphology and mineralization via von Kossa staining up to 35 days. For all of the long-term studies, the stability of the self-assembled PA nanofibers was not a concern because the integrity of the nanomatrix can be maintained up to a month, even with the incorporated enzyme-degradable sequence.<sup>21</sup> Furthermore, it has been shown that differentiated cells produce surrounding ECM that will propagate the continued differentiation

of newly synthesized cells over time.<sup>52</sup> Thus, the ligands inscribed in the PA nanomatrix serve as potential signaling mechanisms for the osteogenic differentiation of hMSCs that can be maintained long-term if the cells are successfully differentiated to produce an ECM microenvironment predisposed to osteogenesis.

Other potential concerns for the long-term osteogenic studies included variations in cell density and protein adsorption on the different PA nanomatrices. It has been reported that a minimum cell attachment threshold is needed to support osteogenic differentiation and mineralization.<sup>31</sup> However, this limitation does not apply because all long-term studies were conducted for at least 7 days, allowing a minimum level of cellularity to be reached. Additionally, the cell densities on all surface conditions were very comparable throughout, thereby negating potential bias caused by differing cell confluencies (Supporting Information, Fig. S2). In regards to protein adsorption concerns, previous literature has shown that self-assembled monolayers are saturated after only 24 hours of incubation over a wide range of serum concentrations.<sup>53, 54</sup> This has been reported on self-assembled monolayers modified with many different surface chemistries, such as  $-NH_2$ ,  $-COOH$ ,  $-CH_3$ , and  $-OH$ .<sup>53-55</sup> Of particular importance is the observed result on  $-OH$  modified surfaces because this correlates directly to PAs, as both display the same terminal chemistry to seeded cells. Therefore, the PA nanomatrix coatings were saturated by the serum within the media before the first time point in all long-term studies. Furthermore, any observed differences in osteogenic differentiation development are most likely attributed to the different ligand interactions presented by the PA nanomatrices and not confounded by disparities in cellularity or protein adsorption.

From this study, the PA-RGDS nanomatrix emerged as the best PA candidate for directing osteogenic differentiation, albeit at an initially slower rate, based solely on ECM-mimicking cell adhesive ligands and without supplemental aid. ALP activity increased significantly over time on PA-RGDS and was found to be much greater on this surface compared to the other PA coatings. In comparison to the hMSCs cultured with OSM, the ALP activity for PA-RGDS did not reach the same levels, indicating an initially slower osteogenic differentiation. The hMSC morphology and mineralization via von Kossa staining were both assessed to further characterize osteogenic differentiation. These evaluations were expanded up to 35 days because the ALP activity results did not indicate later stage mineralization as expected based on past literature, possibly due to the lack of supplemental factors.<sup>27, 56, 57</sup> Characteristic osteogenic morphology progression of spindle-shaped to cuboidal was observed from the hMSCs seeded on the integrin-mediated PA-RGDS nanomatrix in numerous regions throughout the sample coating surfaces, indicating osteogenesis. The von Kossa staining served as validation for these morphological signs of osteogenic differentiation, providing evidence of mineralization. The PA-RGDS nanomatrix displayed significant osteogenic development, as mineralized deposits were detected on days 28 and 35. Furthermore, despite the slower initial osteogenic differentiation based on ALP activity, the observed mineralization on PA-RGDS and with OSM were very comparable after 35 days, indicating a rapid osteogenic maturation on the nanomatrix after the early delay. These findings were enhanced by the quantification of the mineralized areas, as the average size and area percentage of mineral deposition on PA-RGDS was the same as culturing on glass with OSM. PA-DGEA, another integrin-mediated nanomatrix, was the only other PA coating to display instances of osteogenic differentiation, as a few select cuboidal morphologies and positively stained mineralized nodules were observed. No evidence of osteogenic differentiation was detected on the non-integrin binding nanomatrix presented by PA-KRSR, along with the control surfaces of PA-RGES, PA-S, and glass.

Interestingly, integrin-mediated cell binding exerted the greatest influence on controlling cellular behaviors, specifically the RGDS ligand, though the integrin-specific DGEA epitope also proved more effective than the proteoglycan-mediated KRSR ligand. The increased hMSC

attachment on PA-RGDS was expected, as this behavior has been reviewed extensively.<sup>29</sup> Additionally, the observed osteogenic differentiation results were greatly affected by the RGDS ligand-cell interactions. This finding expands upon previous studies that found the RGDS ligand to promote osteogenic development when synergistically combined with supplements<sup>58–60</sup> or without.<sup>27</sup> The negligible results on the control PA-RGES and PA-S conditions validated the RGDS ligand-driven observations, eliminating the potential confounding variables of PA charge and confirmation. Regarding the other PA coatings, the PA-DGEA nanomatrix did display some signs of differentiation. However, it may have a greater impact on mature osteoblast cells, as this ligand signal has been shown to promote integrin-mediated mineralization with fully differentiated osteogenic cells.<sup>61</sup> The proteoglycan-mediated binding presented by the PA-KRSR nanomatrix yielded no evidence of controlling osteogenic differentiation. It appears that the KRSR ligand is only beneficial when utilized in conjunction with other bioadhesive sequences.<sup>62</sup> Taken together, this demonstrates that the RGDS ligand, in the absence of stimulatory factors, leads to the activation of the hMSC signaling responsible for directing osteogenic differentiation by integrin-mediated binding, most likely through the FAK/ERK-mediated pathways.<sup>49, 63</sup>

This research model has potential for broad applications outside of bone regeneration, as it provides fundamental insight into not only understanding essential natural bone tissue formation, but also a new versatile strategy to regenerate a variety of tissues by closely mimicking the principles of natural tissue formation. Furthermore, as a self-assembling biomimetic nanomatrix, the PAs have the capacity to be coated onto other biomedical devices, such as bone fixation implants or cardiovascular stents, functionalizing them with selective bioactivity. Presently, the future plans include designing quantitative real time-PCR gene analysis experiments to detect osteogenic differentiation markers, performing additional positive and negative control experiments with and without osteogenic media supplements to further evaluate possible synergistic effects, investigating composite PA nanomatrices that combine two or more adhesive ligands, and cell encapsulation studies with 3-D self-assembling PA gels. The results from all conducted 2-D studies clearly show that this biomimetic approach allows for osteoprogenitor cells, such as hMSCs, to undergo osteogenic differentiation as directed by nanomatrix scaffolds inscribed with isolated ECM signals.

## Conclusions

Natural tissue formation is a well-organized process that starts at the nanoscale level. Therefore, to best facilitate tissue regenerative needs, a biomimetic approach is needed to capture the complex hierarchical order of native tissue. Focusing on bone tissue regeneration, we have investigated self-assembling PA nanofibers that present ECM-mimicking cell adhesive ligands to specifically tailor the bioactivity and contain functionalized enzyme degradable sites to allow for natural tissue remodeling. This biomimetic construct served as an interface for hMSCs, introduced to provide biological activity. The abilities of the different cell-ligand interactions presented by the PA nanomatrices to influence osteogenic differentiation and other cellular behaviors without the presence of soluble factors were explored. From our studies, the integrin-mediated PA-RGDS nanomatrix was found to have the most promise, demonstrating the importance of integrin-specific binding for osteogenic differentiation. Overall, the incorporation of ECM-mimicking signals, particularly the RGDS ligand, into self-assembling PA nanomatrices is an ideal biomimetic strategy and has great potential for bone tissue regeneration.

## Supplementary Material

Refer to Web version on PubMed Central for supplementary material.

## Acknowledgments

Special thanks to the Biomedical Engineering department at the University of Alabama at Birmingham. The authors gratefully acknowledge Melissa Chimento and the High Resolution Imaging Facility for all TEM imaging. We thank the Mass Spectrometry/Proteomics Shared Facility for analyzing the molecular weights of all samples. Much appreciation is also extended to Jeremy Vines for quantifying the von Kossa mineralization areas. This work was supported by the 2007 Intramural Pilot Grant from the BioMatrix Engineering and Regenerative Medicine Center at UAB and Wallace H. Coulter Foundation awarded to HWJ. Support is also acknowledged from the NIH T32 predoctoral training grant (NIBIB #EB004312-01) for JMA.

## References

1. Daley WP, Peters SB, Larsen M. *J Cell Sci* 2008;121:255–264. [PubMed: 18216330]
2. Kleinman HK, Philp D, Hoffman MP. *Curr Opin Biotechnol* 2003;14:526–532. [PubMed: 14580584]
3. Streuli C. *Curr Opin Cell Biol* 1999;11:634–640. [PubMed: 10508658]
4. Kimelman N, Pelled G, Helm GA, Huard J, Schwarz EM, Gazit D. *Tissue Eng* 2007;13:1135–1150. [PubMed: 17516852]
5. Beniash E, Hartgerink JD, Storie H, Stendahl JC, Stupp SI. *Acta Biomater* 2005;1:387–397. [PubMed: 16701820]
6. Hartgerink JD, Beniash E, Stupp SI. *Science* 2001;294:1684–1688. [PubMed: 11721046]
7. Hosseinkhani H, Hosseinkhani M, Tian F, Kobayashi H, Tabata Y. *Tissue Eng* 2007;13:11–19. [PubMed: 17518577]
8. Huang Z, Sargeant TD, Hulvat JF, Mata A, Bringas P Jr, Koh CY, Stupp SI, Snead ML. *J Bone Miner Res* 2008;23:1995–2006. [PubMed: 18665793]
9. Silva GA, Czeisler C, Niece KL, Beniash E, Harrington DA, Kessler JA, Stupp SI. *Science* 2004;303:1352–1355. [PubMed: 14739465]
10. Stendahl JC, Wang LJ, Chow LW, Kaufman DB, Stupp SI. *Transplantation* 2008;86:478–481. [PubMed: 18698254]
11. Arnold MS, Guler MO, Hersam MC, Stupp SI. *Langmuir* 2005;21:4705–4709. [PubMed: 16032892]
12. Sargeant TD, Guler MO, Oppenheimer SM, Mata A, Satcher RL, Dunand DC, Stupp SI. *Biomaterials* 2008;29:161–171. [PubMed: 17936353]
13. Accardo A, Tesaro D, Mangiapia G, Pedone C, Morelli G. *Biopolymers* 2007;88:115–121. [PubMed: 17154288]
14. Bull SR, Guler MO, Bras RE, Meade TJ, Stupp SI. *Nano Lett* 2005;5:1–4. [PubMed: 15792402]
15. Hosseinkhani H, Hosseinkhani M, Khademhosseini A, Kobayashi H, Tabata Y. *Biomaterials* 2006;27:5836–5844. [PubMed: 16930687]
16. Kim JK, Anderson J, Jun HW, Repka MA, Jo S. *Mol Pharm* 2009;6:978–985. [PubMed: 19281184]
17. Rajangam K, Behanna HA, Hui MJ, Han X, Hulvat JF, Lomasney JW, Stupp SI. *Nano Lett* 2006;6:2086–2090. [PubMed: 16968030]
18. Lowik DWPM, Hest JCMv. *Chem Soc Rev* 2004;33:234–245. [PubMed: 15103405]
19. Stendahl JC, Rao MS, Guler MO, Stupp SI. *Intermolecular Forces in the Self-Assembly of Peptide Amphiphile Nanofibers. Advanced Functional Materials* 2006;16:499–508.
20. Hartgerink JD, Beniash E, Stupp SI. *Proc Natl Acad Sci U S A* 2002;99:5133–5138. [PubMed: 11929981]
21. Jun HW, Yuwono V, Paramonov SE, Hartgerink JD. *Adv Mater* 2005;17:2612–2617.
22. Horii A, Wang X, Gelain F, Zhang S. *PLoS One* 2007;2:e190. [PubMed: 17285144]
23. Hosseinkhani H, Hosseinkhani M, Tian F, Kobayashi H, Tabata Y. *Biomaterials* 2006;27:4079–4086. [PubMed: 16600365]
24. Hosseinkhani H, Hosseinkhani M, Tian F, Kobayashi H, Tabata Y. *Biomaterials* 2006;27:5089–5098. [PubMed: 16782187]
25. Mauney JR, Kirker-Head C, Abrahamson L, Gronowicz G, Volloch V, Kaplan DL. *J Biomed Mater Res A* 2006;79:464–475. [PubMed: 16752403]

26. Na K, Kim SW, Sun BK, Woo DG, Yang HN, Chung HM, Park KH. *Biomaterials* 2007;28:2631–2637. [PubMed: 17331575]
27. Shin H, Temenoff JS, Bowden GC, Zygourakis K, Farach-Carson MC, Yaszemski MJ, Mikos AG. *Biomaterials* 2005;26:3645–3654. [PubMed: 15621255]
28. Pierschbacher MD, Ruoslahti E. *Nature* 1984;309:30–33. [PubMed: 6325925]
29. Hersel U, Dahmen C, Kessler H. *Biomaterials* 2003;24:4385–4415. [PubMed: 12922151]
30. Mardilovich A, Craig JA, McCammon MQ, Garg A, Kokkoli E. *Langmuir* 2006;22:3259–3264. [PubMed: 16548586]
31. Harbers GM, Healy KE. *J Biomed Mater Res A* 2005;75:855–869. [PubMed: 16121356]
32. Balasundaram G, Webster TJ. *J Biomed Mater Res A* 2007;80:602–611. [PubMed: 17031820]
33. Shin H, Jo S, Mikos AG. *Biomaterials* 2003;24:4353–4364. [PubMed: 12922148]
34. Paramonov SE, Jun HW, Hartgerink JD. *J Am Chem Soc* 2006;128:7291–7298. [PubMed: 16734483]
35. Tambralli A, Blakeney B, Anderson J, Kushwaha M, Andukuri A, Dean D, Jun HW. *Biofabric* 2009;1:025001.
36. Palmer LC, Velichko YS, de la Cruz MO, Stupp SI. *Philos Transact A* 2007;365:1417–1433.
37. Harrington DA, Cheng EY, Guler MO, Lee LK, Donovan JL, Claussen RC, Stupp SI. *J Biomed Mater Res A* 2006;78:157–167. [PubMed: 16619254]
38. Storrie H, Guler MO, Abu-Amara SN, Volberg T, Rao M, Geiger B, Stupp SI. *Biomaterials* 2007;28:4608–4618. [PubMed: 17662383]
39. Hasenbein ME, Andersen TT, Bizios R. *Biomaterials* 2002;23:3937–3942. [PubMed: 12162326]
40. Celis JE, Celis A. *Proc Natl Acad Sci U S A* 1985;82:3262–3266. [PubMed: 2860667]
41. Garcia RL, Coltrera MD, Gown AM. *Am J Pathol* 1989;134:733–739. [PubMed: 2565087]
42. Chen DF, Zeng HP, Du SH, Li H, Zhou JH, Li YW, Wang TT, Hua ZC. *Cell Prolif* 2007;40:196–212. [PubMed: 17472727]
43. Semedo P, Palasio CG, Oliveira CD, Feitoza CQ, Goncalves GM, Cenedeze MA, Wang PM, Teixeira VP, Reis MA, Pacheco-Silva A, Camara NO. *Int Immunopharmacol* 2009;9:677–682. [PubMed: 19146993]
44. Mizuno M, Fujisawa R, Kuboki Y. *J Cell Physiol* 2000;184:207–213. [PubMed: 10867645]
45. Kulterer B, Friedl G, Jandrositz A, Sanchez-Cabo F, Prokesch A, Paar C, Scheideler M, Windhager R, Preisegger KH, Trajanoski Z. *BMC Genomics* 2007;8:70. [PubMed: 17352823]
46. Hayashi O, Katsube Y, Hirose M, Ohgushi H, Ito H. *Calcif Tissue Int* 2008;82:238–247. [PubMed: 18305886]
47. Woll NL, Heaney JD, Bronson SK. *Stem Cells Dev* 2006;15:865–879. [PubMed: 17253949]
48. Zhang AX, Yu WH, Ma BF, Yu XB, Mao FF, Liu W, Zhang JQ, Zhang XM, Li SN, Li MT, Lahn BT, Xiang AP. *Mol Cell Biochem* 2007;304:167–179. [PubMed: 17530189]
49. Satija NK, Gurudutta GU, Sharma S, Afrin F, Gupta P, Verma YK, Singh VK, Tripathi RP. *Stem Cells Dev* 2007;16:7–23. [PubMed: 17348802]
50. Ho MH, Hou LT, Tu CY, Hsieh HJ, Lai JY, Chen WJ, Wang DM. *Macromol Biosci* 2006;6:90–98. [PubMed: 16374775]
51. Ho MH, Wang DM, Hsieh HJ, Liu HC, Hsien TY, Lai JY, Hou LT. *Biomaterials* 2005;26:3197–3206. [PubMed: 15603814]
52. Datta N, Holtorf HL, Sikavitsas VI, Jansen JA, Mikos AG. *Biomaterials* 2005;26:971–977. [PubMed: 15369685]
53. Meadows PY, Walker GC. *Langmuir* 2005;21:4096–4107. [PubMed: 15835980]
54. Toworfe GK, Bhattacharyya S, Composto RJ, Adams CS, Shapiro IM, Ducheyne P. *J Tissue Eng Regen Med* 2009;3:26–36. [PubMed: 19012271]
55. Barrias CC, Martins MC, Almeida-Porada G, Barbosa MA, Granja PL. *Biomaterials* 2009;30:307–316. [PubMed: 18952279]
56. Jackson L, Jones DR, Scotting P, Sottile V. *J Postgrad Med* 2007;53:121–127. [PubMed: 17495381]
57. Long MW. *Blood Cells Mol Dis* 2001;27:677–690. [PubMed: 11482883]
58. Behraves E, Mikos AG. *J Biomed Mater Res A* 2003;66:698–706. [PubMed: 12918054]

59. Hu Y, Winn SR, Krajbich I, Hollinger JO. *J Biomed Mater Res A* 2003;64:583–590. [PubMed: 12579573]
60. Yang F, Williams CG, Wang DA, Lee H, Manson PN, Elisseff J. *Biomaterials* 2005;26:5991–5998. [PubMed: 15878198]
61. Xiao G, Wang D, Benson MD, Karsenty G, Franceschi RT. *J Biol Chem* 1998;273:32988–32994. [PubMed: 9830051]
62. Dee KC, Andersen TT, Bizios R. *J Biomed Mater Res* 1998;40:371–377. [PubMed: 9570067]
63. Salasnyk RM, Klees RF, Williams WA, Boskey A, Plopper GE. *Exp Cell Res* 2007;313:22–37. [PubMed: 17081517]

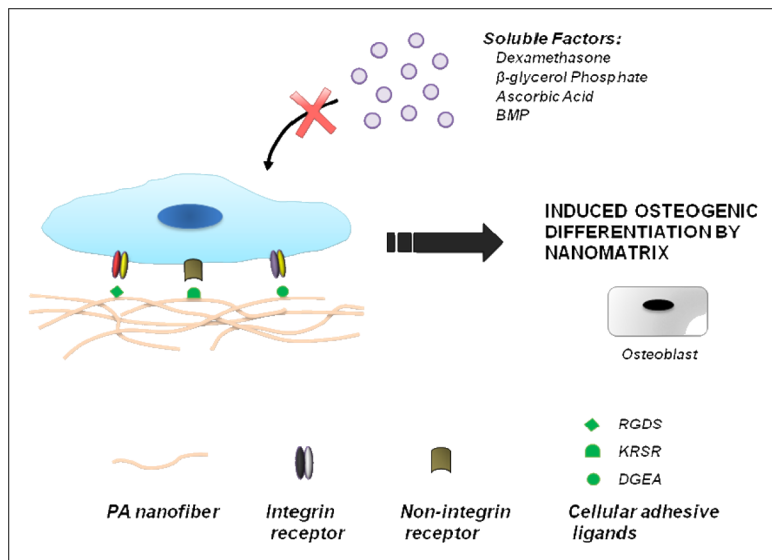


**Figure 1.** Schematic illustration of overall strategy for directing osteogenic differentiation based only on integrin- or non-integrin-mediated binding of specific cellular adhesive ligands incorporated into the PA nanomatrix. No soluble factors were introduced to influence the hMSCs seeded on the PA nanomatrix coatings.

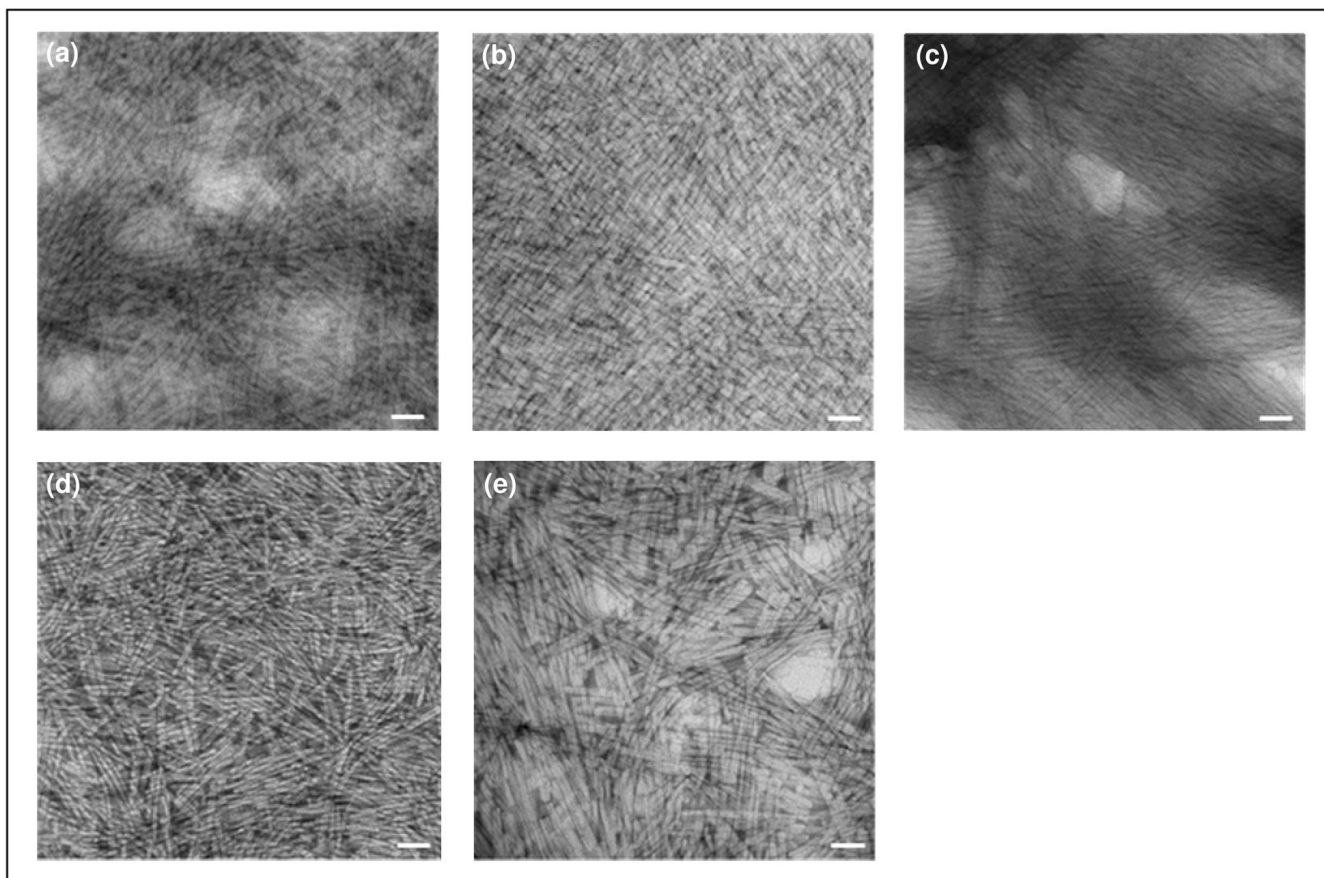


**Figure 2.** TEM images of solvent evaporation induced self-assembled nanofibers that form multilayered PA coatings of (a) PA-RGDS, (b) PA-DGEA, (c) PA-KRSR, (d) PA-RGES, and (e) PA-S. Scale bar represents 40 nm.

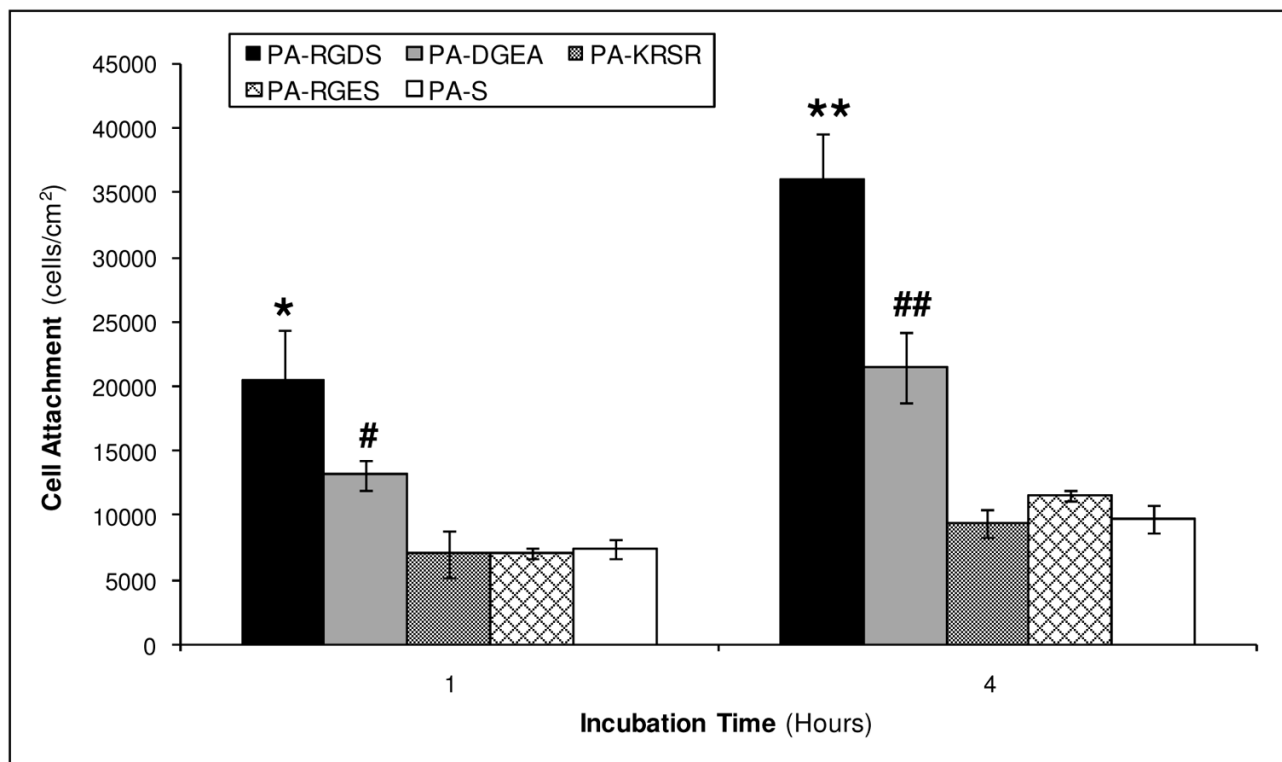


**Figure 3.** Initial attachment of hMSCs on PA coatings. \*, \*\*PA-RGDS promoted significantly greater cell attachment than all other coating conditions after 1 hour and 4 hours ( $p < 0.05$ ). #, ##PA-DGEA promoted significantly greater cell attachment than PA-KRSR, PA-RGES, and PA-S after 1 and 4 hours ( $p < 0.05$ ). Error bar represents mean  $\pm$  standard deviation.

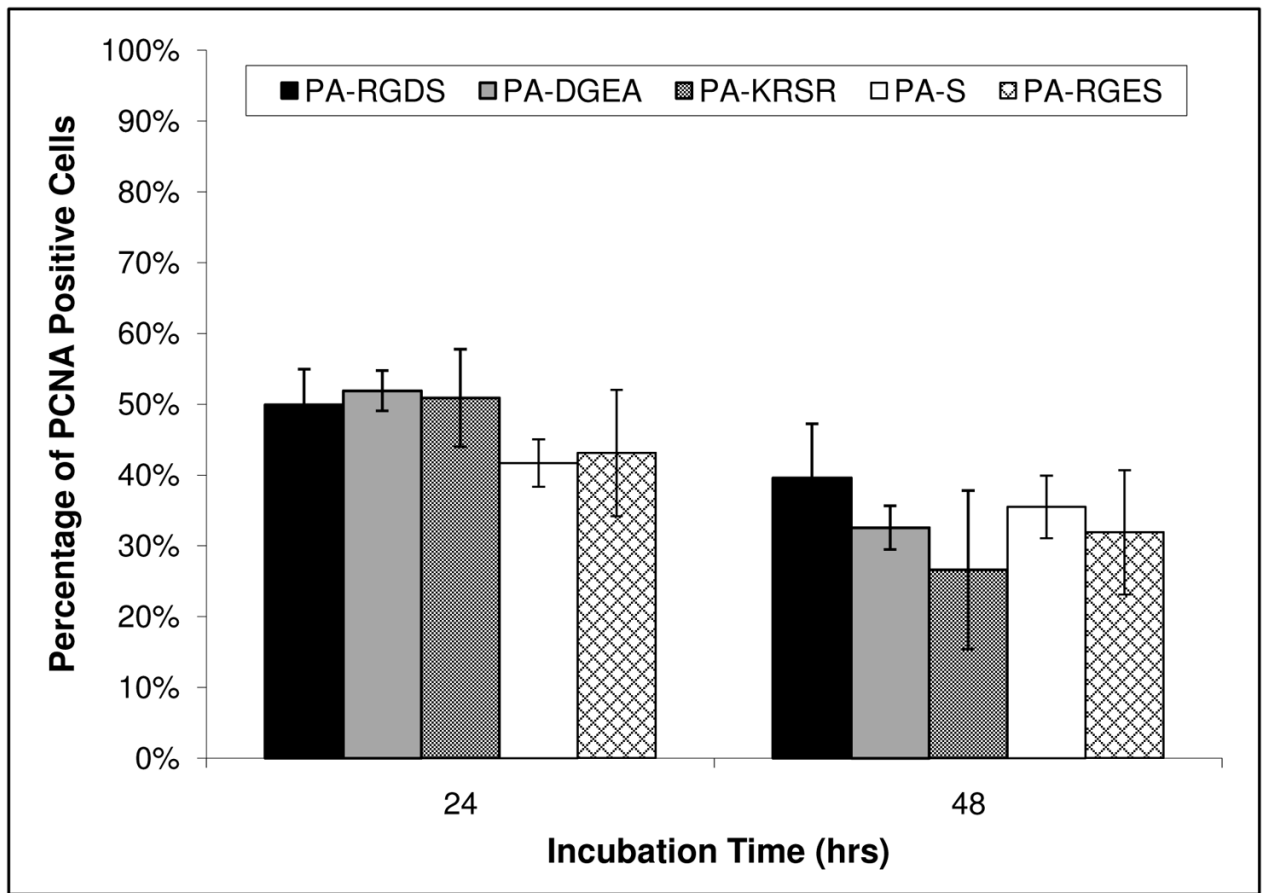


**Figure 4.** Proliferation of hMSCs seeded on the different PA nanomatrix coatings after 24 and 48 hours, quantitatively assessed by PCNA staining. Results are expressed as the percentage of PCNA positive cells. Error bar represents mean  $\pm$  standard deviation.

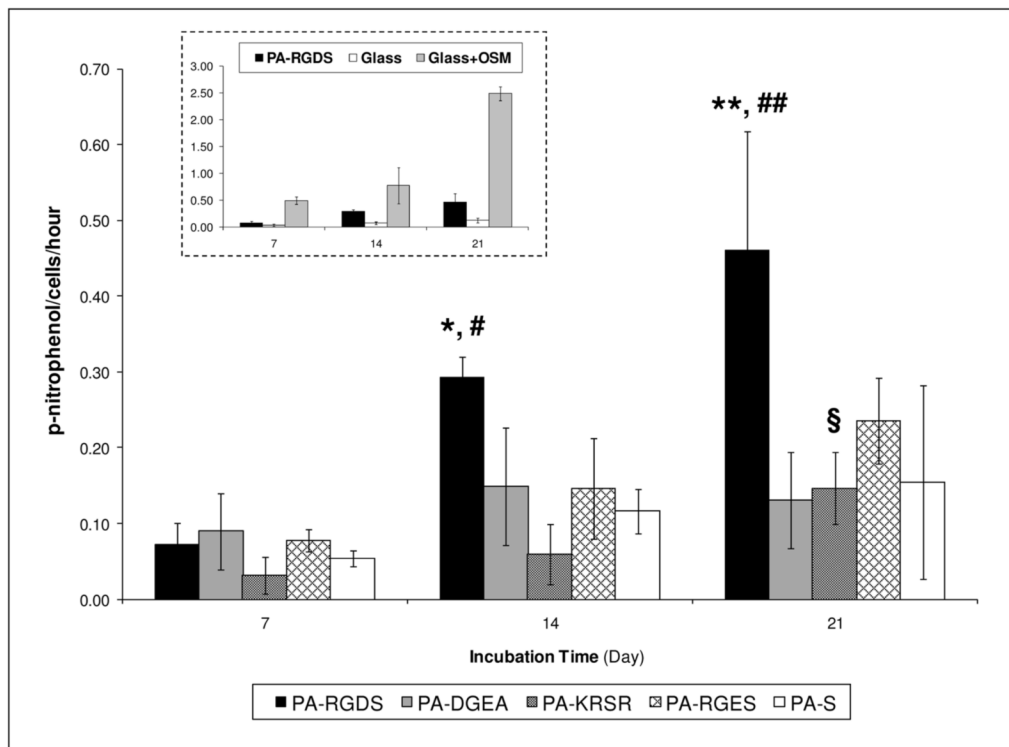


**Figure 5.**

ALP activity of hMSCs on PA nanomatrices. ALP was measured using an end point enzyme assay and results are expressed as p-nitrophenol/cell/hour. \*, \*\*PA-RGDS exhibited significantly more ALP activity than PA-DGEA, PA-KRSR, PA-RGES, and PA-S on days 14 and 21 ( $p < 0.05$ ). #, ##PA-RGDS expressed significantly more ALP activity on days 14 and 21 relative to day 7 ( $p < 0.05$ ). §PA-KRSR showed significantly greater ALP activity on day 21 compared to days 7 and 14 ( $p < 0.05$ ). PA-RGDS in comparison to hMSCs cultured on glass and glass plus osteogenic supplemented media (OSM) is depicted in the top left inset. Error bar represents mean  $\pm$  standard deviation.

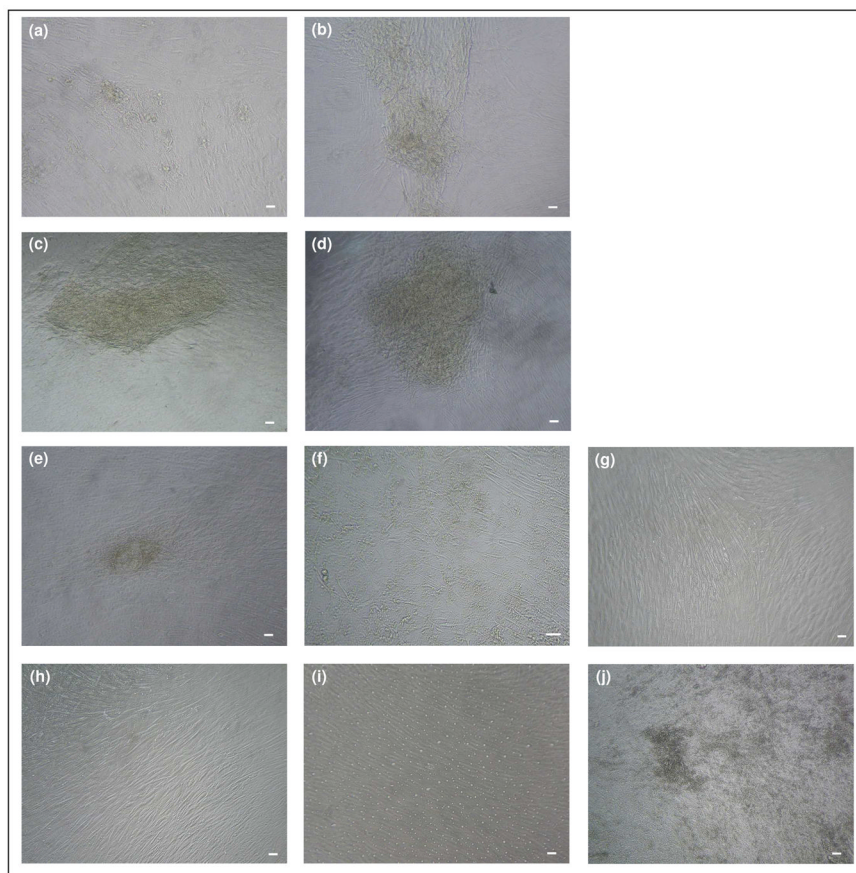


**Figure 6.** Phase contrast images of hMSCs over a long-term incubation period to evaluate osteogenic morphology on PA-RGDS after days (a) 14, (b) 21, (c) 28, and (d) 35. Additional hMSC morphological images provided after 35 days for (e) PA-DGEA, (f) PA-KRSR, (g) PA-RGES, (h) PA-S, (i) glass, and (j) glass plus OSM. Scale bar represents 50  $\mu\text{m}$ .

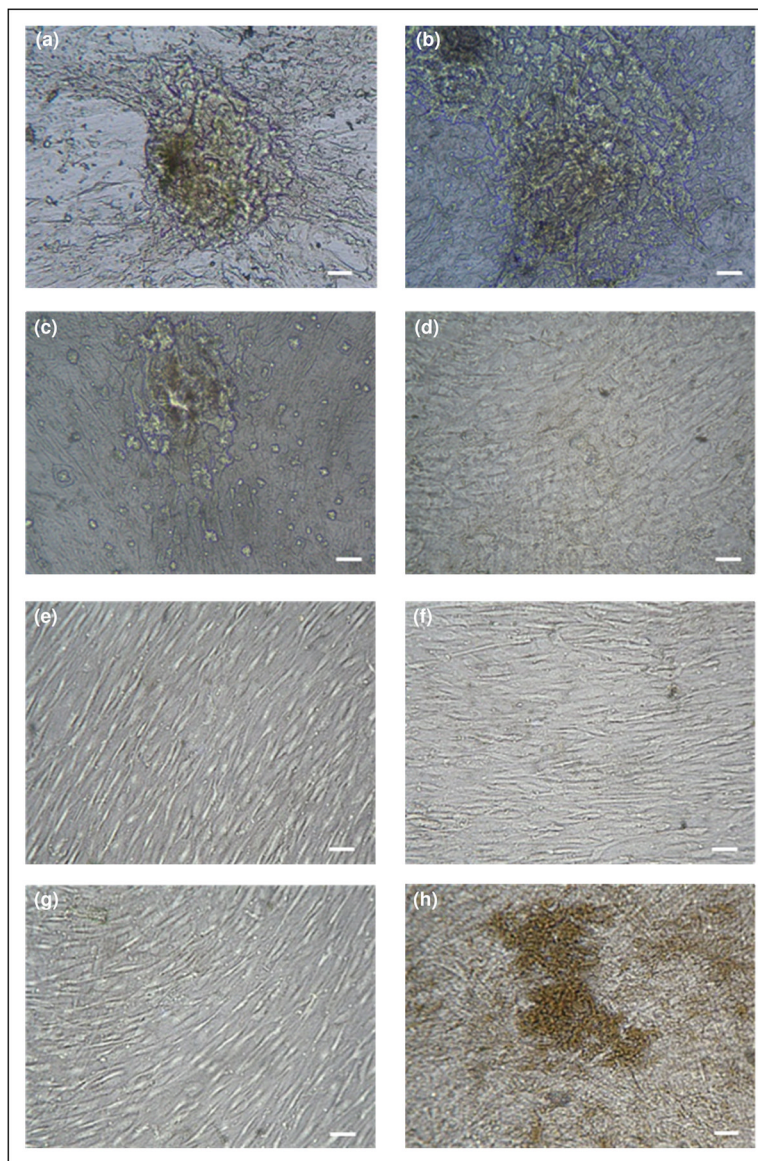


**Figure 7.** Mineral deposition via von Kossa staining of hMSCs on the PA-RGDS nanomatrix after days (a) 28 and (b) 35. Additional von Kossa images after 35 days for (c) PA-DGEA, (d) PA-KRSR, (e) PA-RGES, (f) PA-S, (g) glass, and (h) glass plus OSM. Scale bar represents 50  $\mu\text{m}$ .

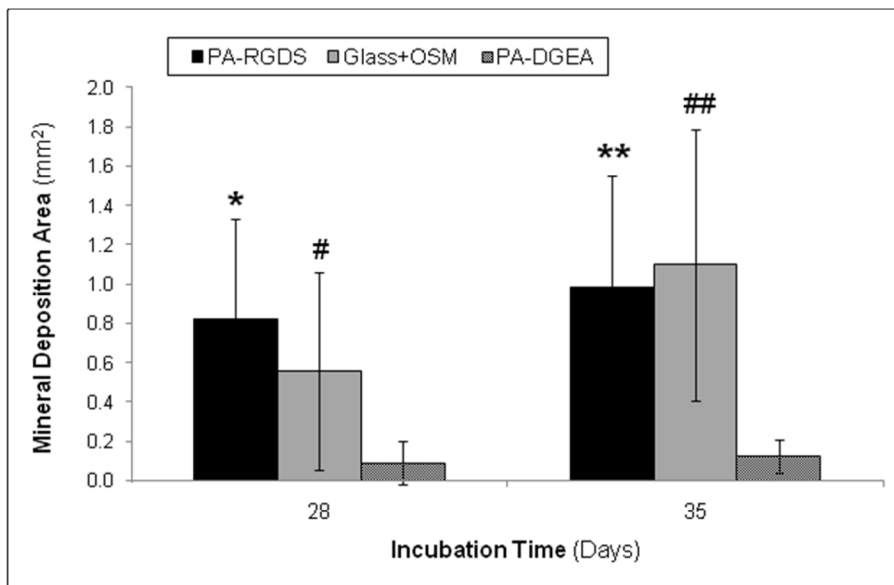


**Figure 8.** Area quantification of the mineralized deposits detected by positive von Kossa staining. \*,\*\*PA-RGDS and #,##glass plus OSM displayed significantly greater mineralized areas than all other coating conditions on days 28 and 35 ( $p < 0.05$ ). Error bar represents mean  $\pm$  standard deviation.

**Table 1**

Peptide amphiphile sequences synthesized

Name	Chemical Sequence	MW <sub>obs</sub> <sup>b</sup>	MW <sub>calc</sub> <sup>c</sup>
PA-RGDS	CH <sub>3</sub> (CH <sub>2</sub> ) <sub>14</sub> CONH – GTAGLIGQ – RGDS	1369.0	1370.0
PA-DGEA	CH <sub>3</sub> (CH <sub>2</sub> ) <sub>14</sub> CONH – GTAGLIGQ – DGEA	1326.8	1326.9
PA-KRSR	CH <sub>3</sub> (CH <sub>2</sub> ) <sub>14</sub> CONH – GTAGLIGQ – KRSR	1481.0	1482.1
PA-RGES <sup>a</sup>	CH <sub>3</sub> (CH <sub>2</sub> ) <sub>14</sub> CONH – GTAGLIGQ – RGES	1383.7	1384.0
PA-S <sup>a</sup>	CH <sub>3</sub> (CH <sub>2</sub> ) <sub>14</sub> CONH – GTAGLIGQ – S	1041.7	1041.8

<sup>a</sup> PA synthesized as a negative control<sup>b</sup> Observed single ion peak for molecular weight<sup>c</sup> Calculated single ion peak for molecular weight